A comparison of cumulus parameterization techniques

By B. F. CESELSKI,[1] *Florida State U., Tallahassee, Fla., USA*

(Manuscript received September 19, 1972)

ABSTRACT

An improved quasi-Lagrangian primitive equation model is used to investigate existing cumulus parameterization schemes. Comparative forty-eight hour forecasts were made utilizing seven different cumulus heating functions, one being zero cumulus latent heat release. Initial data were that of a nondeveloping easterly wave in the Carribbean. Of the six forecasts which included latent heat release, two predictions involving a time-independent vertical heat release function proved to be the most errant. The parameterized heating of Krishnamurti and Moxim, Yamasaki with time-dependent heat release function, convective adjustment, and cumulus scale mass conservation, produced comparable results. Time mean maximum ascending motions of the four similar forecasts ranged from a low of -2×10^{-4} mb sec^{-1} with Krishnamurti & Moxim heating to a high of near -6×10^{-4} mb sec^{-1} for Yamasaki heating. Convective adjustment and cumulus scale mass conservation techniques tended to produce poorer low-level forecasts because of a strong dependency upon the initial moisture distribution. Concurring results among forecasts were consistent with the previous tropical scale analysis of Charney. For the easterly wave of moderate intensity, computed vertical motions indicated essentially no coupling of upper and lower tropospheric motion outside convective areas and only minimal coupling in regions of cumulus latent heat release. Seventy to eighty percent of the ascending motion and eddy kinetic energy produced within the wave was estimated to be the direct result of parameterized cumulus latent heat release.

1. Introduction

Recent numerical weather prediction studies in the tropics have essentially agreed on one point; the desire and need to include the effects of cumulus clouds in tropical forecasting. The cumulus latent heating function, H_c, in the thermodynamic equation is seen below:

$$\frac{\partial \theta}{\partial t} + u\frac{\partial \theta}{\partial x} + v\frac{\partial \theta}{\partial y} + \omega\frac{\partial \theta}{\partial p} = +\frac{H_c}{C_p}(P_0/p)^{R/C_p} + \dots \quad (1.1)$$

Symbols are defined below.[2]

[1] Presently affiliated with the National Center for Atmospheric Research, Boulder, Colorado. The National Center for Atmospheric Research is sponsored by the National Science Foundation.

[2] *List of symbols*

a	percent area of active cumulus clouds
C	cumulus scale mass flux from boundary layer
c_p, C_p	specific heat capacity of air at constant pressure
D	boundary constant of Mintz-Arakawa general circulation model
E	total static energy
E_a	adjusted total static energy
E_B	static energy of prediction model boundary layer
E_{BDY}	static energy of general circulation boundary
E_c	static energy of a cumulus cloud
E^*	saturated total static energy
H_c	diabatic heating by cumulus convection
I	moisture convergence
L	latent heat of evaporation
M	moisture sources and sinks
PR	reference pressure at which adjusted energy is conserved
p_B	cloud base pressure (900 mb)
p_T	cloud top pressure (100 mb)
Q_1	moisture convergence required to raise environmental temperature
Q_2	moisture convergence required to raise environmental humidity
q_s	saturation mixing ratio
T	temperature in degrees absolute
t	time
z	heights of pressure surfaces above 1 000 mb
z_s	height of pressure surfaces of saturated air
λ	saturated vertical moisture gradient parameter
Δt	cloud time scale
η	entrainment parameter
θ	potential temperature
ω	vertical velocity, dp/dt
ω^*	vertical velocity at boundary layer top

The formulation of H_c is complicated by several factors. One problem is that when cumulus clouds are most likely to exist, the synoptic scale atmosphere is conditionally unstable; i.e.,

$$-\frac{\partial}{\partial p}(gz + C_pT) > 0$$

$$-\frac{\partial}{\partial p}(gz + C_pT + Lq) < 0.$$

The usual latent heating function for the stable atmosphere, $H = -L\omega(\partial q_s/\partial p)$, gives rise to a computational instability when applied to the conditionally unstable atmosphere (Krishnamurti, 1968). The computational instability encountered simply reflects the fact that the tropical atmosphere is not stable for large scale layer-ascent. Another complicating factor arises from the small horizontal scale of cumulus clouds relative to the typical grid resolution possible with available computers. Consequently, since the stable heating function is inappropriate and cumulus phenomena are on a subgrid scale, one must formulate or parameterize a new heating function in terms of the larger, observable scales of atmospheric processes.

Several dissimilar cumulus parameterization procedures have been developed by research groups working on a wide range of projects. Each procedure developed has differed typically in a way dictated by convenience and the type of problem and integration model involved. Most existing parameterization schemes can be classified into three general categories.

(a) *Parameterizations related to moisture convergence*

The first group, referred to here as type A, is composed of schemes in which the cumulus heating is assumed to be proportional to the total moisture convergence or vertical motion at the boundary layer top. This type of parameterization originated mainly with the works of Charney & Eliassen (1964) and Ooyama (1964) and is the most widely adopted technique. Extensive usage of this method has led to several related but not identical techniques.

Most schemes in this group allow the cumulus heating to be released as a function of time and space, and are primarily dependent upon the temperature difference of the model cloud and cloud environment. In some cases, however, a vertical distribution of latent heat release is specified for all time such that heating takes place continuously and does not cease if the environment becomes warmer than the cloud. Consequently, considerably more heat can be released by the latter method. In addition to those cited above, type A parameterizations have been proposed in studies by Kuo (1965), Krishnamurti (1968), Krishnamurti & Moxim (1971), Ooyama (1969), Yamasaki (1968*a*, *b*, *c*; 1969), and Rosenthal (1969).

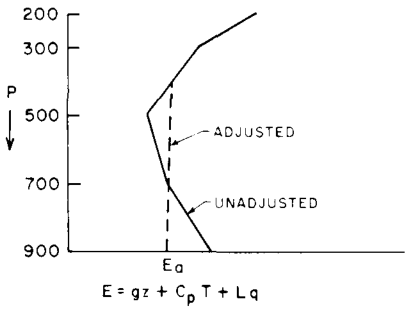

Fig. 1. Sketch of convective adjustment.

(b) *Convective adjustment technique*

The second type of parameterization, type B, has stemmed mainly from general circulation studies. The method is somewhat simpler in theory and application than type A, and consequently, more convenient in terms of computing time and storage requirements for long-period integrations. The method is applied when the model atmosphere is computed to be conditionally unstable and the stable heating function cannot be used unless the conditional instability is first removed. Cumulus overturning is assumed to take place instantaneously such that the conditionally unstable portion of the atmosphere is replaced by a cumulus cloud, i.e., the moist adiabatic lapse rate. The constraint that the total adjusted static energy, $E_a = (gz + C_pT + Lq)$, of a grid point be equal to the vertical integral of the unadjusted static energy, is placed to prevent a spurious energy loss or gain due to adjustment. A basic difference from type A is that the adjustment of the entire sounding takes place instantaneously; whereas type A adjustment applies only to a small percent ($\approx$ 1 %) of the mass in a grid cell. Furthermore, since type B conserves energy during adjustment, energy input into the integration box actually takes place by enhanced surface fluxes of sensible and latent heat that restore the energy to the low levels which was redistributed upward in the previous adjustment. Type A, on the other hand, treats the boundary layer as the energy source and adds energy directly to higher levels during adjustment.

(c) *Cumulus scale mass conservation technique*

The third category, type C, involves the concept of mass continuity on the cumulus scale (Arakawa, 1969). The procedure is that if some mass flux is computed to rise moist adiabatically within a cloud, a compensating negative mass flux subsides outside the cloud. In this parameterization, heating occurs both as latent heat release to the upper level and as compensating subsidence at all levels. Space and time occurrence of convection also differ with types A and B in that amounts of heating are determined by static energy $(gz + C_pT + Lq)$ distributions. When the low-level static energy supply becomes large, energy is released through convection to the upper layers in a prescribed relaxation time, τ. The conditional instability of the model atmosphere is removed in relaxation time τ, if energy is not resupplied to the boundary layer by synoptic scale convergence or by surface fluxes. Shallow convection is also parameterized in a way similar to deep convection, but primarily as a method of transporting moisture from the boundary layer into the lower one-half of the atmosphere. No latent heat is imparted directly to the environment although subsidence heating is taken into account.

The effect of type C convection on the total energy $(gz + C_pT + Lq)$ distribution is similar to that produced by type B convection. The cumulus scale mass conservation technique tends to conserve total energy during overturning, although with this scheme the adjustment applies only to a small percent of the mass at a grid point. In the overturning, mass with large values of energy is transported from the boundary layer to the upper levels. The boundary layer high-energy mass is replaced by lower-energy mass which subsides from above. Energy input into the integration box is primarily the result of surface fluxes of sensible and latent heat, as is the case in type B convection.

(d) *Characteristics of the three general types of model convection*

(1) Horizontal distribution of heating:
(*a*) Type A convection occurs at a grid point if there is mass convergence in the boundary layer.

(*b*) Type B convection occurs at a grid point if the model atmosphere is computed to be conditionally unstable and the relative humidity is greater than 100 % (boundary layer convergence may be either positive or negative.)

(*c*) Type C convection occurs if the boundary layer static energy exceeds the moisture saturated static energy of the uppermost layer (boundary layer convergence may be either positive or negative.)

(2) Vertical distribution of heating:
(*a*) Type A convection extends upward to 100 mb but heating occurs only if the cloud temperature exceeds the environment temperature at a particular level. Heating is achieved through direct mixing of cloud with environment.

(*b*) Type B convection extends upward only to a level for which energy is conserved for the adjustment. The top of the adjusted layer may be 500 mb or lower. Sensible heating may occur from the conversion of latent heat in the adjusted layer or as stable heating throughout the trophosphere if the model atmosphere is convectively stable and the air is rising.

(*c*) Type C heating extends throughout the troposphere as dry adiabatic subsidence outside the cloud and also occurs in the upper troposphere through direct mixing.

(3) Moisture sources and sinks:
(*a*) Type A convection adds moisture directly to the environment at all levels through cloud-environment mixing. The boundary layer is an infinite latent heat reservoir.

(*b*) Type B convection may either add or deplete environment moisture at a particular level. A source or sink is determined by the mixing ratio of the adjusted sounding (moist adiabat) being greater or less than the environment mixing ratio before adjustment.

(*c*) Type C convection is almost totally a moisture sink at all levels because of the dry adiabatic subsidence outside the cloud. A small moisture source does exist ar the uppermost level where cloud-environment mixing takes place.

(4) Static energy sources:

(*a*) Type *A* convection assumes the boundary layer to be an infinite energy reservoir and the model clouds add energy to the integration box from the reservoir.

(*b*) Type *B* convection exactly conserves energy during adjustment. Energy input into the integration box takes place through the enhancement of surface fluxes of sensible and latent heat. The surface itself is the energy reservoir in this case.

(*c*) Type *C* convection nearly conserves energy during cumulus overturning. Energy input into the integration box is primarily determined by enhanced surface fluxes. As in type *B* convection, the surface is the energy reservoir.

Using one prediction model and the same set of initial data, comparative 48-hour forecasts are made. The results of these predictions have shed some light on the advantages and disadvantages of a particular scheme and, of equal importance, how the schemes are interrelated.

Various aspects of the seven forecasts are discussed in relation to the dynamics of the easterly wave. To date, diagnostic studies and a very limited number of numerical weather prediction experiments in the tropics have resulted in an unclear definition of the synoptic scale systems which are observed in low latitudes. Previous studies have differed substantially in their conclusions as to the types and magnitudes of synoptic scale vertical motions, sources of kinetic energy, and the importance of cumulus clouds and their interaction with the larger scale tropical systems.

Although the seven heating functions employed in this study defined a wide range of heat input possibilities, some properties of the wave were predicted quite similarly. Several schemes produced related forecasts of a reasonably good quality. This fact suggests that the predicted quantities which showed agreement among schemes were, indeed, representative of the true wave.

2. The comparative prediction experiments

In all, seven separate 48-hour forecasts were made using a different cumulus heating funcion in each. One experiment was run with no latent heat release, while the remaining six experiments utilized five separate heating parameterizations. Two forecasts were made with variations of the same scheme.

(a) *Experiment 1, no cumulus heating*

The first forecast was made with H_c in Eq. (1.1) equal to zero. The object of this experiment was to help isolate the effects of cumulus convection in the remaining experiments. Results of this experiment were compared quantitatively with the results of each of the forecasts made with $H_c \neq 0$.

(b) *Experiment 2, Krishnamurti & Moxim*

Experiment 2 was essentially that of Kuo (1965) with revisions of Krishnamurti (1968) and Krishnamurti & Moxim (1971). Four basic assumptions of the scheme were outlined by Kuo:

(1) Convection occurs in regions where low-level moisture convergence is positive, and the stratification is conditionally unstable.

(2) Surface or boundary layer air is the source of a deep cloud whose essential character can be represented by a moist adiabat.

(3) Vertical extent of the cloud is from a low level of condensation to a height where the moist adiabat of the cloud again crosses the environment temperature profile. For simplicity in the prediction model, the condensation level is assumed to be 900 mb. All clouds extend upward to 100 mb.

(4) Cumulus clouds exist only momentarily, afterward mixing totally with the environment.

Heating for the conditionally unstable portion of the atmosphere is defined by:

$$
\begin{aligned}
H_c &= c_p \frac{a}{\Delta t}(T_s - T); \quad && \omega^* < 0;\ T_s > T \\
H_c &= 0 \quad && ;\ \omega^* \geqslant 0 \text{ or } T_s < T \qquad (2.1)
\end{aligned}
$$

$(T_s - T)$ represents the temperature difference between the cloud element and cloud environment; c_p is the specific heat capacity at constant pressure; Δt is the cloud time scale, and a is a measure of the percent area of the grid cell covered by active cumulus clouds. The vertical motion (ω^*) is that of the boundary layer top (900 mb). The parameter, a, is obtained as a ratio of the actual moisture convergence out of the boundary layer to the moisture convergence required to fill the entire three-dimensional grid cell with convective cloud.

$$a = \frac{Q_1 + Q_2}{I} \tag{2.2}$$

$$Q_1 = \frac{1}{g\Delta t}\int_{P_B}^{P_T} \frac{C_p}{L}(T_s - T)\,dp$$

$$Q_2 = \frac{1}{g\Delta t}\int_{P_B}^{P_T} (q_s - q)\,dp$$

Q_1 represents the condensed portion of the moisture convergence required to raise the environment temperature to saturated cloud temperature, and Q_2 is the moisture convergence necessary to raise the environment mixing ratio to cloud saturated mixing ratio. $I = -(\omega^* q/g)$ is the computed low-level moisture convergence. Net moisture convergence, as originally defined by Kuo (1965), included lateral convergence at levels above the boundary layer top.

$$I = \frac{1}{g}\int_{P_B}^{P_T} (\nabla q V)\,dp - \frac{\omega^* q}{g}$$

Revisions of the scheme by Krishnamurti (1968) included the dropping of the first term on the right hand side as a second-order effect in comparison to the upward flux from the boundary layer.

If the model atmosphere is computed to be conditionally unstable and moisture convergence is positive, a percent area (a) of deep cumulus clouds rises to 100 mb and mixes completely with the environment. The moisture source, M, due to mixing is given by

$$M = \frac{a(q_s - q)}{\Delta t}$$

(c) *Experiment 3, Yamasaki (1968c)*

The Yamasaki heating function is closely related to that in the previous experiment, yet contains some subtle and important differences. The modeled cloud is essentially that involved in Krishnamurti & Moxim heating with the basic assumptions of that experiment applying in this scheme as well. Cumulus latent heating is defined as,

$$H_c = -c_p(P/P_0)^{R/c_p} h(p)\, S\omega^*; \quad \omega^* < 0,\ T_s > T$$

$$H_c = 0 \qquad ; \ \omega^* \geqslant 0 \text{ or } T_s < T \tag{2.3}$$

where

$$S \equiv -\frac{\partial \theta}{\partial p}$$

and

$$h(p) = \frac{Lq^*}{c_p S}(P_0/P)^{R/c_p} \frac{(T_s - T)}{\int_{P_B}^{P_T} (T_s - T)\,dp}$$

The variable, S, has been introduced so that h becomes nondimensional, and h may be viewed as a vertical heating distribution function. In this experiment, h was variable and computed at each grid point and time step when the vertical motion at the boundary top, (ω^*), was less than zero. In Experiments 4 and 5, h was treated as a parameter and held constant for the entire forecast.

For comparison with Experiment 2, Eq. (2.3) reduces simply to

$$H_c = -Lq^*\,\omega^* \frac{(T_s - T)}{\int_{P_B}^{P_T} (T_s - T)\,dp} \tag{2.4}$$

Equation (2.4) is identical with Eq. (2.1) except for two factors: (1) the pressure integral of $(q_s - q)$ does not appear in the denominator and corresponds to $Q_2 = 0$ in Eq. (2.2); and (2) mixing ratio at the boundary layer top (q^*) is constant, whereas this quantity is a predicted variable in the Krishnamurti–Moxim parameterization. These two differences, especially (1), lead to a substantially different heating function. Under normal tropical conditions, $\int(q_s - q)\,dp$ dominates $\int(T_s - T)\,dp$ such that the Yamasaki heating does not correlate exactly in space with that of Experiment 2 and tends to have a magnitude two or more times that of Experiment 2.

Moisture was not a predicted variable of the Yamasaki hurricane models, and consequently no lateral mixing of moisture between cloud and environment was defined.

(d) *Experiment 4, Yamasaki (1968a, 1969)*

The cumulus heating function of Experiment 3 was simplified by specifying the vertical heat release distribution function (h) as being a prescribed parameter. The heating function was simply

$$H_c = -c_p(P/P_0)^{R/c_p} h(p)\, S(x,y,p)\, \omega^*(x,y); \quad \omega^* < 0$$

$$H_c = 0 \quad ; \quad \omega^* \geq 0$$

The vertical distribution of latent heating is almost totally determined by h, since spatial variations of S provide only a secondary amount of variation.

Although he recognized this to be an extremely simple heating function, Yamasaki (1968*a*) assumed the representation to be adequate in describing some general dynamics of the hurricane. Of more importance to this paper was the inclusion of a similar heating function (Yamasaki, 1969), in a study of tropical wave instabilities. The above heating function was instrumental in defining what meteorological modes were computed as being most unstable in the tropics; e.g. the easterly wave was found to exist for profiles which included $h(p)$ less than or equal to unity in low levels. With data containing a moderate easterly wave, it was thought of interest to apply an h profile indicative of the unstable easterly wave mode found by Yamasaki. The object of this forecast was to test applicability of this simple heating function in the broader context of tropical prediction in general. A heating profile of $h(700) = 1.0$, $h(500) = 2.0$, and $h(300) = 3.0$ was adopted in this experiment, and the profile resembled closely that described by Yamasaki for which the easterly wave should exist.

There was some reason to question the validity of the simplified heating function. In the scheme, there is no cessation of heating when the environment temperature reaches a specific cloud temperature, and unconditional heating occurs provided that $\omega^* < 0$. The result is total heating considerably larger than that described by a variable heating distribution function.

(e) *Experiment 5, Yamasaki (1968, 1969)*

Experiment 5 was identical to Experiment 4 except that the specified heating distribution function was $h(700) = 3.0$, $h(500) = 1.5$, and $h(300) = 0.0$. This forecast was run primarily because of the results obtained in Experiments 2 and 3. As will be discussed in detail in the following sections, it was found that for the given data, both the Krishnamurti–Moxim & Yamasaki (1968) schemes released almost all heat to the lower and middle troposphere. The ratio of heat released at 700 mb to heat released at 500 mb was about 2 to 1.

It previously had been recognized that the simplified form ($H_c \propto -hS\omega^*$) releases large amounts of heat. By specifying $h(p)$ in a manner related to the results of Experiments 2 and 3, one obtained a reasonable heating profile and included the maximum amount of heat release allowable with schemes thus far developed.

(f) *Experiment 6, convective adjustment*

The convective adjustment technique used in this experiment was not that of any particular research group but had been developed specifically for input data levels corresponding to the integration model. In principle, the method was very similar to that described by Manabe et al. (1965) and Washington & Kasahara (1970).

Although convective adjustment techniques vary somewhat from one research group to the next, the requirement of total static energy ($gz + c_pT + Lq$) conservation during adjustment greatly limits the differences in techniques. The technique used in this experiment incorporated the energy conservation restriction. The method of obtaining the adjusted sounding which conserved total energy followed closely that described by Krishnamurti & Moxim (1971). The procedure however, is too involved to describe with sufficient detail in this text.

Convective adjustment does not add total energy to the system, but merely redistributes total energy in the vertical and alters energy forms between latent and internal. Convectively stable latent heat release or large-scale condensation is also included as a further process whereby latent energy is converted to internal energy. In general circulation studies the normal procedure is to apply large-scale condensation when the relative humidity tends to exceed 100 % and the grid point has not convectively adjusted. The procedure typically used is an iterative process whereby the excess moisture is condensed and the corresponding released latent heat added to the environment. The stable heating used in this experiment is, $H = -L\omega\,(\partial q_s/\partial p)$, and has the same effect as the iterative method, i.e., it converts the excess moisture into sensible heat.

Convective adjustment is allowed to take

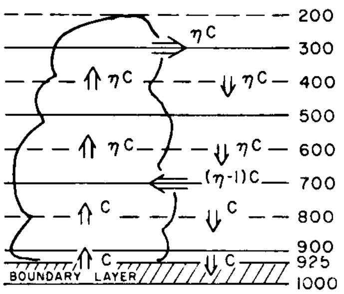

Fig. 2. Cloud model of the cumulus scale mass conservation technique. C is the upward mass flux from the boundary layer; $(\eta-1)\,C$ is the entrainment if $\eta>1$; ηC is the total in-cloud mass flux after entrainment.

place only if the atmosphere is conditionally unstable, relative humidity at 900 mb is greater than 100 %, and vertical motion is less than zero at 900 mb. Stable heating occurs if the grid point has not been adjusted, relative humidity is greater than 100 %, and the local p-velocity is less than zero.

(g) *Experiment 7, cumulus heating with cloud scale mass conservation*

The parameterization method employed here was basically that developed by Arakawa (1969) and incorporated in part the alterations of the technique made by Langlois & Kwok (1970). Some further changes were necessitated by dissimilarities in the Mintz-Arakawa general circulation model and the experiment model. The fundamental concepts of mass conservation in deep convection, and cumulus-overturning occurring as a function of the vertical distribution of total static energy, however, were followed in this experiment.

Fig. 2 represents cumulus scale mass conservation for deep cumulus clouds. C is the upward mass flux from boundary layer into the cloud; $(\eta-1)\,C$ is the horizontal mass flux from environment to cloud ($\eta>1$ represents entrainment); and ηC is total upward mass flux in the cloud after entrainment. Differences from the original approach stem primarily from the definition of the boundary layer. The Mintz-Arakawa model carries moisture at only one low level and the boundary layer is assumed to be infinitesimally thin. For convenience, the top of the boundary layer for this experiment was defined to be 925 mb.

Cloud energy after entrainment is

$$E_c = E_{700} + \frac{1}{\eta}(E_{\mathrm{BDY}} - E_{700})$$

Following Langlois & Kwok, η is specified as being unity; i.e., neither entrainment nor detrainment occurs. E_c is equal to the boundary energy (E_{BDY}) since E is essentially conserved for moist adiabatic motion. At 300 mb

$$E_c = c_p T_{c300} + g z_{300} + L q^*(T_{c300}) \tag{2.12}$$

where q^* is saturation specific humidity. One can also define

$$E^*_{300} \equiv c_p T_{300} + g z_{300} + L q^*(T_{c300}) \tag{2.13}$$

By combining (2.12) and (2.13), an expression for temperature difference between cloud and environment at 300 mb is obtained:

$$T_{c300} - T_{300} = \frac{1}{1+\lambda_{300}}\frac{1}{c_p}(E_c - E^*_{300}) \tag{2.14}$$

where

$$\lambda_{300} \equiv \frac{L}{q}\left(\frac{\partial q^*}{\partial T}\right)_{300}$$

For a cloud to have positive buoyance at 300 mb ($T_c > T$), $E_c = E_{\mathrm{BDY}}$ must be larger than E^*_{300}, and consequently $E_{\mathrm{BDY}} \geqslant E^*_{300}$ is the criterion for occurrence of deep penetrating convection.

Equation (2.14), together with subsidence outside the cloud, determines the 300-mb heating function,

$$H_c = \frac{Cg}{\Delta p}\left[\frac{1}{1+\lambda_{300}}(E_c - E^*_{300}) + c_p(P/P_0)(\theta_{300} - \theta_{400})\right]$$

The moisture source M at 300 mb is

$$M = \frac{Cg}{\Delta p}\left[q^*_{300} + \frac{\lambda_{300}}{1+\lambda_{300}}\frac{1}{L}(E_c - E^*_{300}) - q_{400}\right]$$

Since no mixing of cloud and environment is assumed to take place below 300 mb, all heat and moisture sources below are simply defined by dry adiabatic subsidence of mass flux ($-C$). Levels below 300 mb are then heated and dried if deep convection occurs.

The mass flux, C, is obtained by Langlois & Kwok by assuming that, in the absence of a large scale energy replenishment and allowing

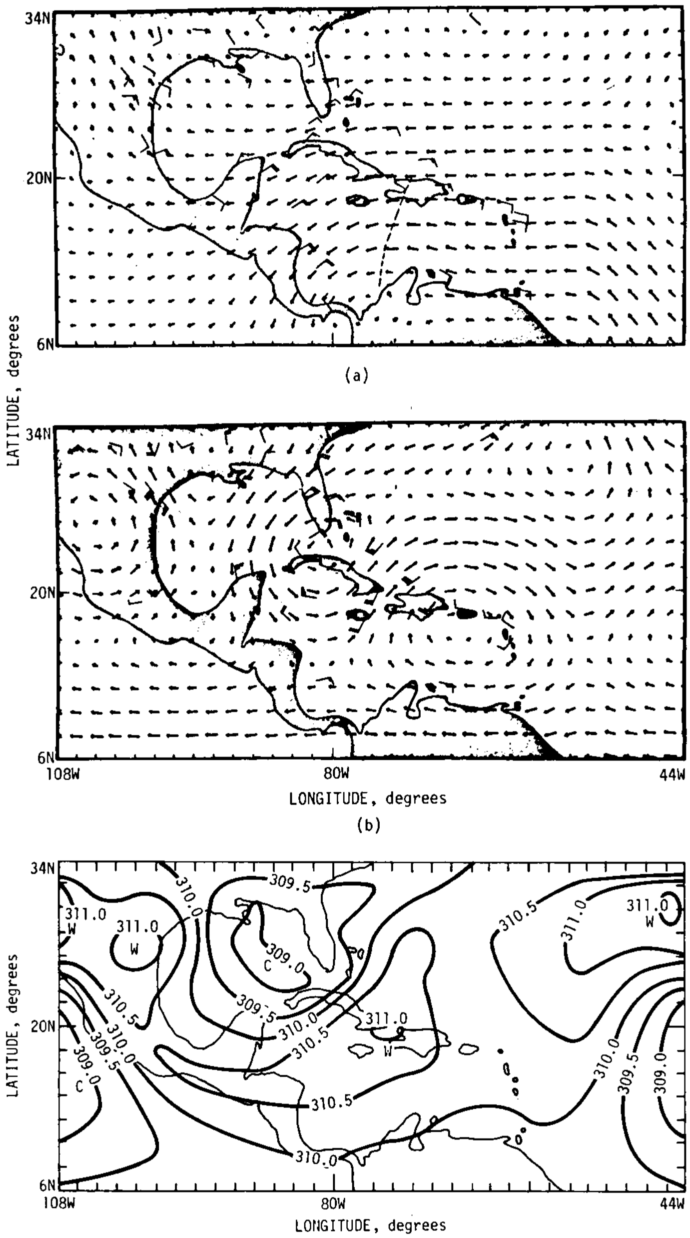

Fig. 3. Initial wind fields at (*a*) 1 000 mb and (*b*) 200 mb. Observed wind barbs are in knots and balanced wind vectors are in meters per second (←equivalent to 10 m sec^{-1}). (*c*) Initial potential temperature field at 700 mb. Isotherm interval is 0.50 degrees.

no other diabatic energy source, cumulus overturning will reduce energy differences between the boundary and 750 mb in a specified amount of time, τ. In the general circulation model the cloud scale mass flux is derived to be

$$C = \frac{\Delta P}{g\tau} \frac{[E_{\mathrm{BDY}} - E^*_{750}]}{(1-D)\,[(E^*_{750} - E^*_{250})/(1+\lambda_{250}) + S_{250} - S_{500}]/ + (1+\lambda_{750})\,(S_{500} - c_p T_{\mathrm{BDY}})} \tag{2.15}$$

where $S \equiv gz + c_p T$ and D is a small constant (≈ 0.01). Using a boundary top of 925 mb and the prediction levels of the present model, Eq. (2.15) was approximated for Experiment 7 by

$$C = \frac{\Delta P}{g\tau} \frac{E_{925} - E^*_{700}}{(E^*_{700} - E^*_{300})/(1+\lambda_{300}) + S_{300} - S_{500}/ + (1+\lambda_{700})(S_{500} - c_p T_{925})}$$

Shallow convection, although treated similarly to deep convection by Arakawa, has been modified considerably in this experiment. If $E_B > E^*_{700}$, but $E_B \leqslant E^*_{300}$, such that deep convection is not present, then shallow convection is included only as a process of transporting moisture from the boundary layer to 700 mb. No latent heat is released, and mass is not conserved in the overturning. The only effect of shallow convection is to offset the strong drying tendency deep convection produces at 700 mb.

3. Initial data and prediction model

The data set chosen for the comparative forecasts is that previously used in the diagnostic studies of Krishnamurti & Baumhefner (1966). The data grid is a 2° longitude by 2° latitude mesh covering the area of 6–34° N and 56–108° W. Included in the area is an easterly wave of moderate intensity and an upper-tropospheric cold-core low. Figs. 3*a*, *b*, and *c* show initial 1 000- and 200-mb windfields and 700-mb potential temperature field, respectively. Maximum wave intensity is in the low levels and the system does not develop in time. The choice of a nondeveloping system is intentional in that the interest is in viewing a wide range of parameterization techniques. It was felt that data involving a developing tropical system might add extra departure to the forecasts not necessarily desired. In particular, the convective adjustment method is not intended to be applicable in tropical storm development, but it is still assumed to be capable of simulating tropical dynamics in general.

Krishnamurti & Kanamitsu (1972) also examine this wave in some detail.

The prediction model used is essentially that defined by Krishnamurti et al. (1972). Some minor changes were necessary to accomodate the different heating function employed in each forecast. No forecast in this study utilizes the heating function of Krishnamurti & Kanamitsu (1972) and consequently no work has been repeated. Each forecast described in the following section is necessarily different because of the heating function defined for that experiment.

4. Results depicting variability among schemes

The results of the seven 48-hour predictions can be divided into predicted quantities which showed definite variation among schemes and quantities, generally of a larger scale, that were predicted similarly. With the exception of Experiments 4 and 5 where the very simple heating function was used, the gross features predicted in each experiment are quite similar. Predicted 48-hour height fields of Experiments 1, 2, 3, 6 and 7 vary among themselves by only 5–10 metres at any particular grid point. Concurring results are discussed in section 5.

An example of the type of forecast obtained is that of Experiment 2 (Krishnamurti & Moxim heating). Figs. 4*a* and 4*b* depict the 36-hour predicted wind fields with the actual observed wind barbs superimposed. Observed cyclonic and anticyclonic centers are predicted quite well at 200 mb while agreement at 1 000 mb is somewhat less. The forecast is understandably less desirable near the north and south constant-height walls. Other schemes predicted motion fields similar to that of Experiment 2 except for Experiment 4 where overdevelopment occurred in mid-levels and Experiment 5 which overdeveloped the low-level easterly wave. Fig. 5*c* is the 36-hour field of potential temperature at 700 mb for Experiment 2. Most schemes produced a similar low-level temperature field. The low-level wave was generally forecast as being relatively warm west of the axis and cooler east of the axis.

To facilitate the determination of the influence of the heating function within the easterly wave, the computation box in Fig. 5 was chosen. The box is centered on the 1 000-mb vorticity maximum with the intention of obtaining east–west cross-sections of quantities through the most intense portions of the wave. Figs. 6–12 are (x,p) crossections, where quantities are first averaged along 10° of latitude and then a time mean computed for 36 hours (forecast hours 12–48). The first 12 hours of prediction

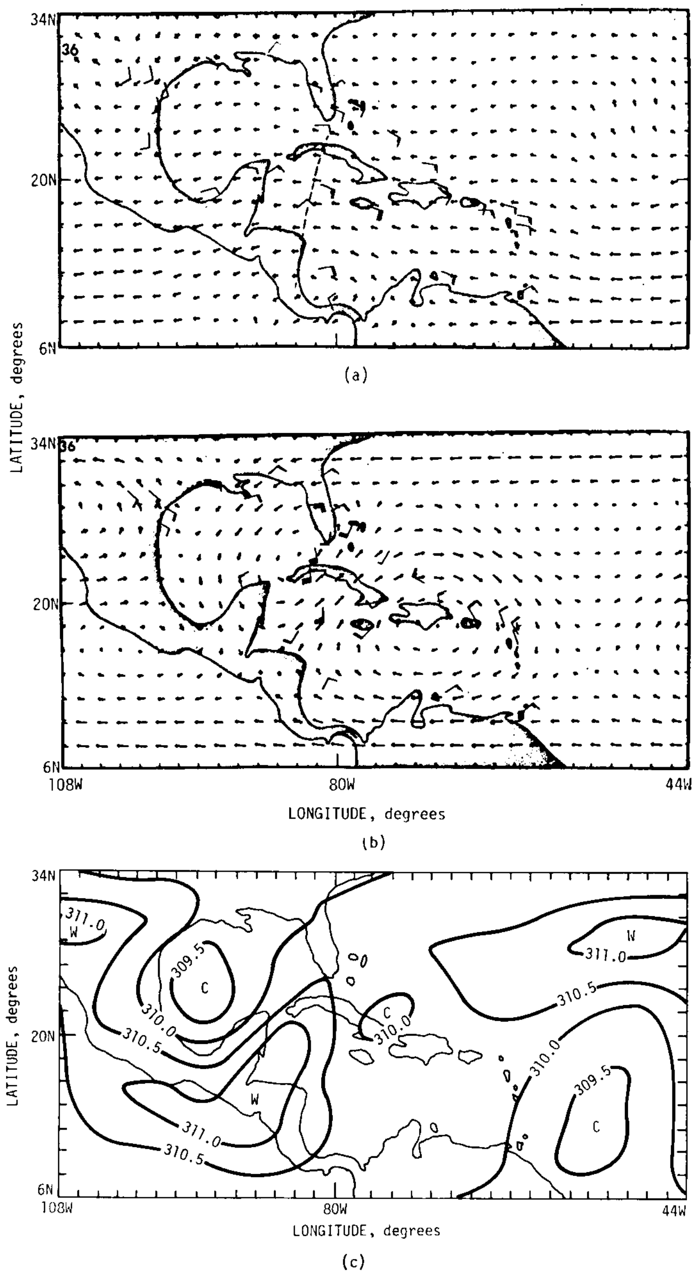

Fig. 4. Forecast wind fields of Experiment 2 at 36 hours with observed wind barbs superimposed at (*a*) 1 000 mb and (*b*) 200 mb. The scale is identical to that of Fig. 4. (*c*) Predicted 36-hour potential temperature at 700 mb for Experiment 2. Isotherm interval is 0.50 degrees.

time have been omitted to lessen the effect of initial oscillations. The upper Figs. of 6–12 are mean vertical motions, while the lower represents a temperature deviation from the model mean at the corresponding level; again averaged in latitude and time.

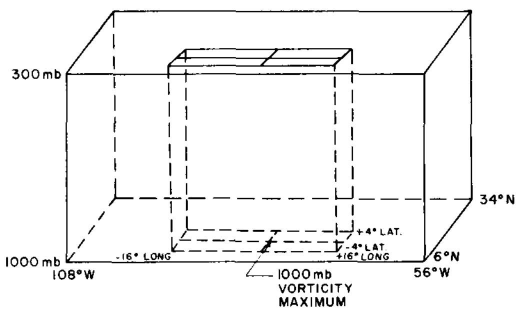

Fig. 5. Computational box centered on the 1 000-mb vorticity maximum; extending over 34° longitude and 10° latitude.

(a) (x,p) *cross-sections of* ω

Experiment 1 (Fig. 6*a*): Of immediate notice when no latent heat is released is that the rising motion, when averaged in y and t, is very small in magnitude and essentially splits two large subsidence cells to the east and west. Rising motion extends upward only to 700 mb, tilting west to east with height. All rising motion at 1 000 mb and 900 mb is confined to the area of maximum vorticity and to the west of it. Upper and lower tropospheric vertical motions appear uncoupled. The rising motion at 200 mb is likely related to the cold low aloft.

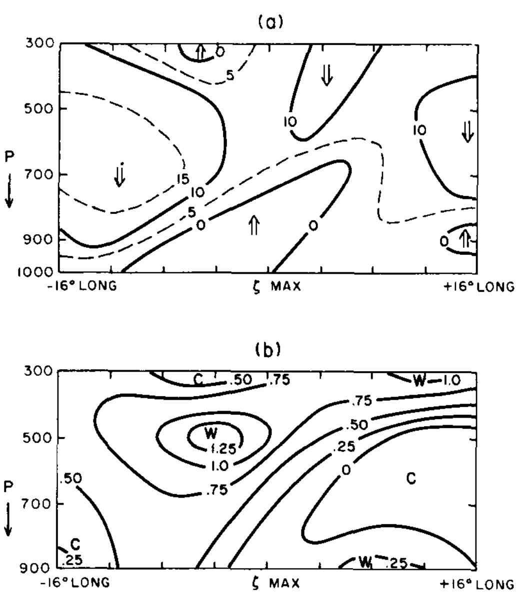

Fig. 6. For no cumulus heating, (x, p) cross-sections of (*a*) vertical motion and (*b*) temperature deviation from pressure level mean of full grid. All quantities are averaged over 10° latitude and 36 forecast hours. Isopleth intervals are 10×10^{-5} mb sec^{-1} (intermediates of 5×10^{-5} mb sec^{-1}) in (*a*) and 0.25° in (*b*).

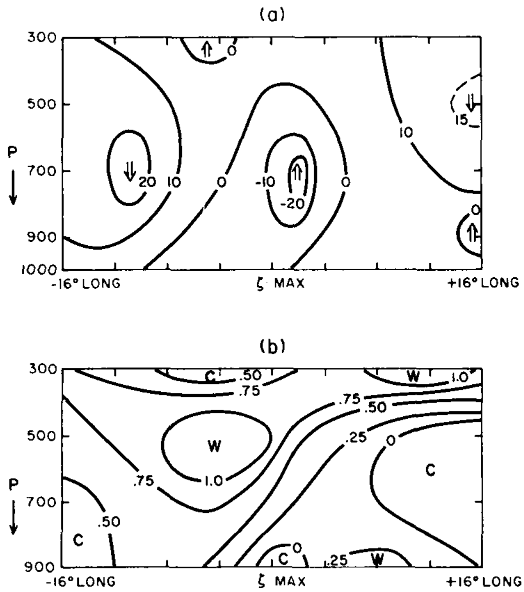

Fig. 7. For Krishnamurti & Moxim heating, cross-sections of (*a*) vertical motion and (*b*) temperature deviation (see Fig. 7, legend). Isopleth interval of 10×10^{-5} mb sec^{-1} (intermediates of 5×10^{-5} mb sec^{-1}) in (*a*) and 0.25° in (*b*).

Experiment 2 (Fig. 7*a*): Rising motions with Krishnamurti & Moxim heating are much larger than with no heating. Maximum ascending motion occurs behind the vorticity maximum at 700 mb and is reflected downward to 900 mb even though no latent heat is released at that level in the experiment. Negative omega extends up to 500 mb but apparently is subdued at 300 mb by the sinking tendency of the upper-level depicted in Fig. 6*a*. Subsidence is slightly intensified in the western cell.

Experiment 3 (Fig. 8*a*): As expected, Yamasaki heating ($h = h(x, y, p, t)$) was considerably stronger than that of Krishnamurti & Moxim. Mean rising motion, although having nearly the same location in space, has a magnitude of about three times that of Experiment 2. The rising motion does not extend upward to 300 mb as subsidence prevails there.

Experiment 4 (Fig. 9*a*): Yamasaki heating, ($h(p) = 1.0, 2.0, 3.0$), by definition releases large amounts of heat to upper levels. Reflecting the

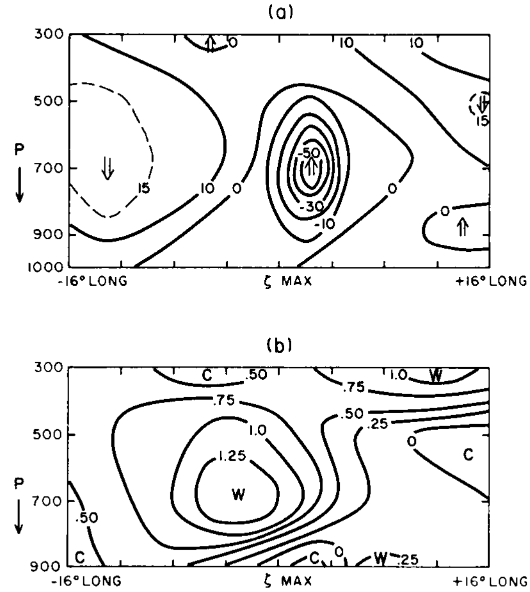

Fig. 8. For Yamasaki ($h = h(x, y, p, t)$) heating, cross-sections of (a) vertical motion and (b) temperature deviation (see Fig. 7, legend). Isopleth intervals are 10×10^{-5} mb sec^{-1} (intermediates of 5×10^{-5} mb sec^{-1}) in (a) and 0.25° in (b).

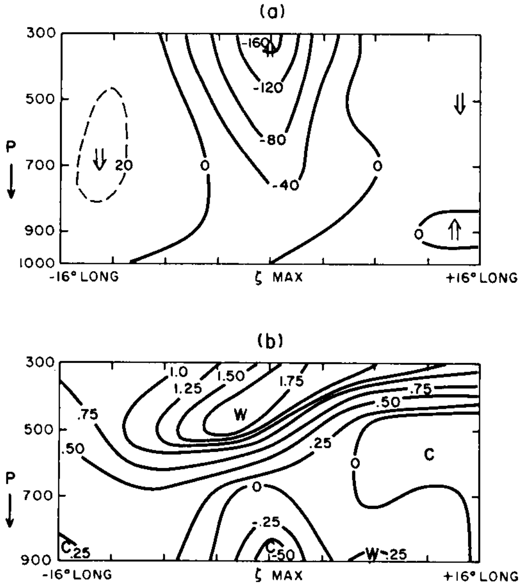

Fig. 9. For Yamasaki $h(p) = 1.0,\ 2.0,\ 3.0$) heating, cross-sections of (a) vertical motion and (b) temperature deviation (see Fig. 7, legend). Isopleth intervals are 40×10^{-5} mb sec^{-1} (intermediates of 20×10^{-5} mb sec^{-1}) in (a) and 0.25° in (b).

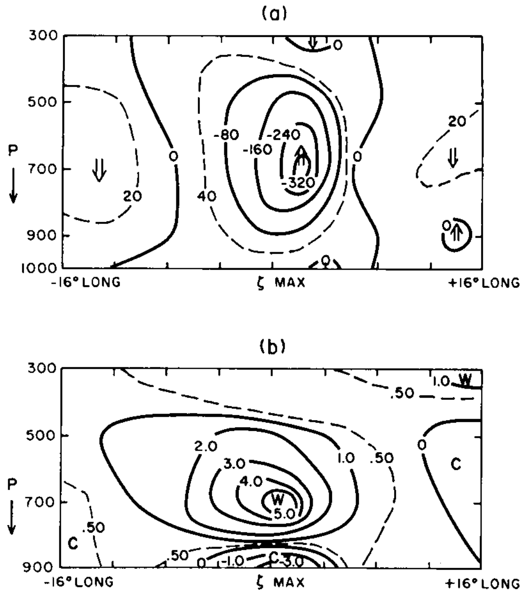

Fig. 10. For Yamasaki $h(p) = 3.0,\ 1.5,\ 0.0$) heating, cross-sections of (a) vertical motion and (b) temperature deviation (see Fig. 7, legend). Isopleth intervals of 80×10^{-5} mb sec^{-1} (intermediates of 40×10^{-5} and 20×10^{-5} mb sec^{-1}) and 1.0° in (b).

large heating are rising motions at 300 mb nearly an order of magnitude larger than the 700 mb maximum of Experiment 2. The subsidence tendency at 300 mb over the wave axis is completely overwhelmed. The rising motion at low-levels remains tilted as in the previous experiments. Subsidence is again intensified slightly in the western cell.

Experiment 5 (Fig. 10a): Yamasaki heating, ($h(p) = 3.0,\ 1.5,\ 0$), was defined to primarily heat the low-levels and vertical motion produced at 700 mb exceeds that produced by Krishnamurti & Moxim heating by more than an order of magnitude. These vertical motions, as well as those of the previous experiment, tend to be excessive and indicate overheating.

Experiment 6 (Fig. 11a): The vertical motions of convective adjustment are comparable in magnitude to those of Experiments 2 and 3, but are now displaced toward the east. This displacement is due to large low-level moisture values in the initial data extending well east of the wave axis. Since the scheme is dependent directly on static energy stability rather than low-level moisture convergence, it is possible for heating to be displaced if maximum instability does not fall exactly behind the wave axis.

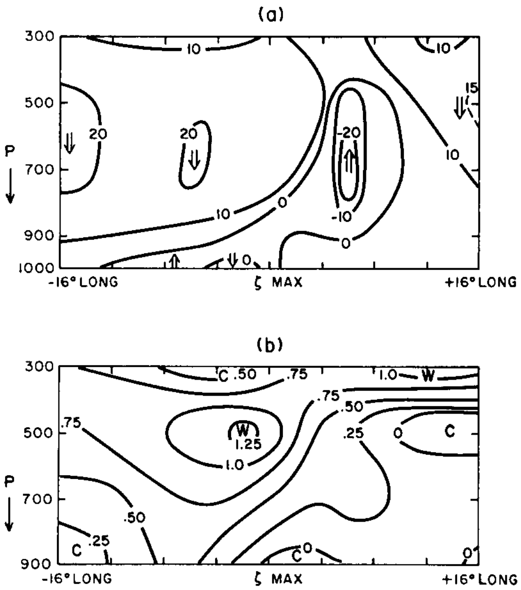

Fig. 11. For convective adjustment, cross-sections of (*a*) vertical motion and (*b*) temperature deviation (see Fig. 7, legend). Isopleth intervals of 10×10^{-5} mb sec^{-1} (intermediates of 5×10^{-5} mb sec^{-1}) in (*a*) and 0.25° in (*b*).

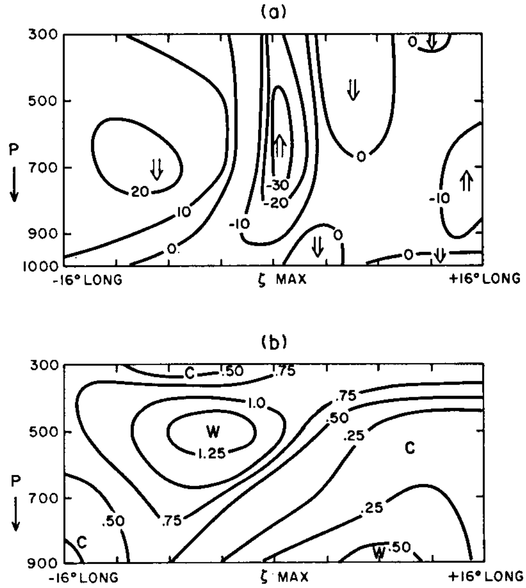

Fig. 12. For cumulus scale mass conservation heating, cross-sections of (*a*) vertical motion and (*b*) temperature deviation (see Fig. 7, legend). Isopleth intervals of 10×10^{-5} mb sec^{-1} in (*a*) and 0.25° in (*b*).

Experiment 7 (Fig. 12*a*): Cumulus scale mass conservation leads to heating and vertical motion related to that of convective adjustment. Maximum rising motion in this case occurs exactly at the vorticity maximum; however, as in Experiment 6, heating and rising motion occur over a considerable distance east of the wave axis. Similar to convective adjustment, this scheme is related closely to static energy profiles and heating does not necessarily fall immediately behind the wave axis. Also of interest is the observation that heating and vertical motion extend throughout the entire vertical column since all convection extends to high levels and cumulus scale subsidence heats all levels below. A necessary coupling of high and low tropospheric synoptic scale motion is implied. The remaining parameterization techniques however, do not, by definition, distribute heat uniformly in the vertical, and therefore vertical motions may or may not be coupled.

(b) *(x,p) cross-sections of temperature deviations from model mean*

In general, mean temperature deviations from the corresponding pressure-level mean tend to strongly reflect the position where cumulus heating has taken place and vertical motion was produced. Fig. 6*b* indicates a basic pattern of relatively cool temperatures tilting from the low-level wave axis eastward with height. Lying above and parallel to the cool axis is a large warm anomaly. These patterns are hydrostatically consistent with that of Riehl (1954), whose classic wave tilts eastward with height. Figs. 7*b*–12*b* deviate from Fig. 6*b* mainly by displacing the maximum warm anomaly toward the point of maximum heating. The extremes of this are Experiments 4 and 5.

Even though Experiments 2 and 3 are closely related, the additional heating involved in the Yamasaki scheme, ($h = h(x, y, p, t)$), has been sufficient to lower the maximum positive anomaly from 500 mb in Experiment 2 to 700 mb in Experiment 3.

Dry adiabatic lifting of environment air has produced cold anomalies below the level of maximum heating in Experiments 2–5. Since no latent heat is released at 900 mb, rising motion produced by latent heat input at the level above leads to adiabatic cooling. Experiment 4 (Fig. 9*b*) has produced a cold-core disturbance up to 700 mb where obviously dry adiabatic ascent was dominating the cumulus latent heat release there. Experiment 6 (Fig. 11*b*) also produced the cold core at 900 mb, but in this case was the result of the convective adjustment effect rather than adiabatic cooling. In Experiment 7 (Fig. 12*b*), the adiabatic cooling at 900 mb is apparently overshadowed by the cumulus scale subsidence heating at that level.

(c) *Kinetic energy and energy exchanges*

Conversion of eddy available potential energy to eddy kinetic energy for each forecast was computed using the following:

$$[\mathrm{PE}\cdot\mathrm{KE}] = -\frac{R}{g}\int_{100}^{1000}\frac{\overline{\omega' T'}}{P}\,dp \qquad (4.1)$$

The cyclic east-west boundaries allowed the conversion rates to be computed for each two-degree latitude interval. Computed exchanges were then averaged over 36 forecast hours (hours 12–48) to give time mean zonally-averaged conversion rates (Figs. 13*a* and *b*).

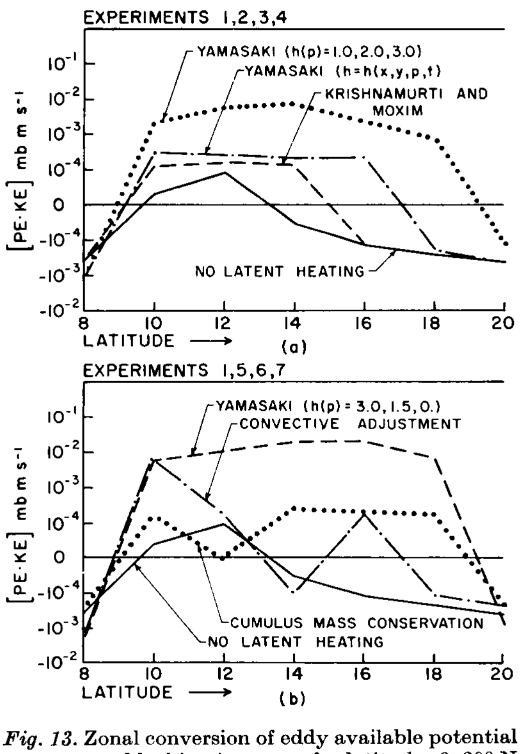

Fig. 13. Zonal conversion of eddy available potential energy to eddy kinetic energy for latitudes 8–20° N Experiments 1, 2, 3, and 4 depicted in (*a*) and 1, 5, 6, and 7 in (*b*). The scale is linear between powers of 10 and all values represent the 36 hour time mean (forecast hours 12–48) for the particular latitude.

Table 1. *Thirty-six hour (forecast hours 12–48) mean eddy kinetic energy for full grid. Units of* $m^2\ s^{-2}$.

Experiment No.; heating function	Mean eddy kinetic energy
5; Yamasaki ($h(p) = 3.0,\ 1.5,\ 0.$)	6.262
4; Yamasaki ($h(p) = 1.0,\ 2.0,\ 3.0$)	5.010
7; Cumulus mass conservation	4.030
6; Convective adjustment	3.894
3; Yamasaki ($h = h(x, y, p, t)$)	3.706
2; Krishnamurti & Moxim	3.585
1; No cumulus heating	3.529

All rates, including that of no latent heating, show that available eddy potential energy was converted to eddy kinetic energy in the southern portion of the grid where the easterly wave had maximum intensity. Rates of eddy kinetic energy production reflect closely the vertical motions of Figs. 6*a*–12*a*. Experiments 4 and 5 again stand out. The large heating in these two forecasts produced strong vertical motion and converted substantial amounts of potential energy to kinetic energy. Production of eddy kinetic energy was clearly smallest in the case of no cumulus latent heat release.

Experiment 3 heating produced more eddy kinetic energy than Experiment 2, but the conversion rates of Experiments 2, 3, 6 and 7 are of a related magnitude. Conversion rates north of 20° N showed no significant variation among schemes and have not been depicted.

Thirty-six hour time mean eddy kinetic energy for the full integration grid is listed in Table 1. Mean eddy kinetic energy of Experiments 4 and 5 well exceed the others, while the experiment with no latent heating contained the least. The relative position of Experiment 6 is somewhat deceptive, however, in that a significant quantity of eddy kinetic energy existed in the $(2\Delta X)$ wavelength and did not necessarily indicate stronger eddy motions within the easterly wave. The $(2\Delta X)$ energy of Experiment 6 apparently stemmed from an individual grid point being adjusted while the surrounding points remained unadjusted or had not been adjusted recently.

One major shortcoming of the prediction model is the tendency to destroy eddy motions in time. The imposition of walls within close

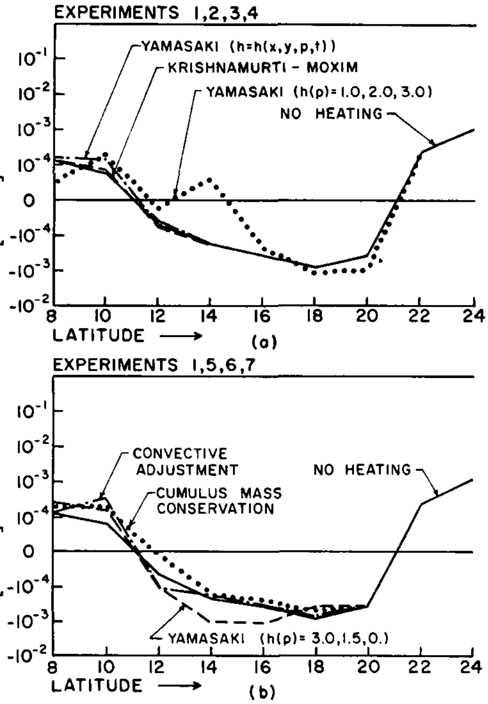

Fig. 14. Zonal conversion of zonal kinetic energy to eddy kinetic energy for latitudes 8–24° N, depicted as in Fig. 14.

proximity to the disturbance has the effect of weakening the system. Consequently, the numbers in Table 1 can represent only relative quantities of eddy kinetic energy among forecasts and cannot be used to compare with the verification data to see which scheme has best predicted the observed eddy motion.

The conversion of zonal kinetic energy to eddy kinetic was computed using,

$$[\mathrm{KZ}\cdot\mathrm{KE}] = -\frac{1}{g}\int_{100}^{1000}\left(\overline{u'v'}\frac{\partial \bar{u}}{\partial y} + \overline{\omega' u'}\frac{\partial \bar{u}}{\partial p}\right)dp \quad (4.2)$$

Figs. 14*a* and *b* are the 12–48 hour time mean conversions plotted at two-degree latitude intervals.

Conversions of zonal to eddy kinetic energy are quite similar among forecasts and show much less variation than [PE·KE] conversions. Consequently, schemes which produced more eddy kinetic energy in Fig. 13 tend to show the larger mean existing eddy kinetic energy of Table 1.

The large production of eddy kinetic energy at 12° N in Fig. 13 apparently leads to a conversion of the opposite sign in Fig. 14. Large amounts of eddy kinetic energy are being converted to zonal kinetic energy with the maximum occurring one or two grid points north of the maximum intensity of the wave.

The absolute values of conversion rates plotted in Figs. 13 and 14 will be discussed further in the following section.

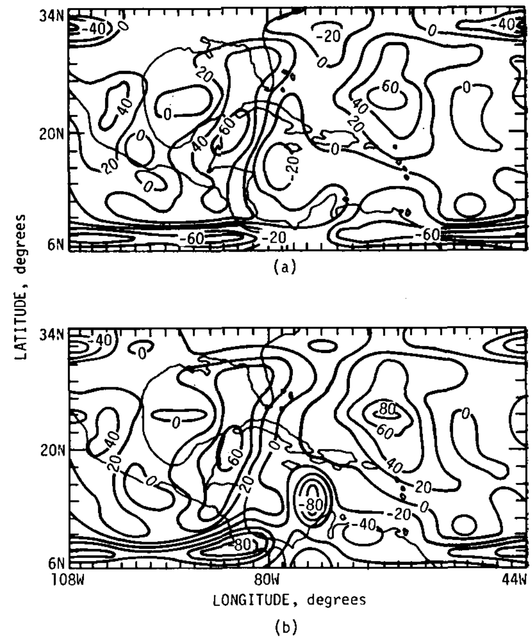

Fig. 15. Vertical velocity at 700 mb at forecast hour 18 (*a*) for Experiment 1 and (*b*) for Experiment 3. Isopleth interval is 20×10^{-5} mb sec^{-1}.

5. Results depicting agreement among schemes

Charney (1963) used scale analysis to suggest that in the absence of strong cumulus convection, the tropics were dominated by quasi-nondivergent motions. Scaling indicated that for non-convective regions, vertical motion in the tropics must be much smaller than in extratropics for the same velocity, length and stability scales.

Results of the seven comparative forecasts substantiate Charney's theory. This is seen by the extremely small mean values of vertical motion in Fig. 6*a*, and in Figs. 7*a*–12*a* outside the area of maximum rising motion associated with latent heat release. Time mean vertical motions without latent heat release are found on the order of $1-2 \times 10^{-4}$ mbs^{-1} while unaveraged values are of the order of $4-8 \times 10^{-4}$ mbs^{-1}. Fig. 15*a* shows vertical velocity with no cumulus heating at forecast hour 18. The field is typical of map times after initial oscillations subside.

Shukla (1969), in a tropical numerical experiment containing no convective heating, obtained vertical motions on the order of 10^{-4} to 10^{-3} mb sec^{-1}. The weat descending motion of the non-convective refions predicted in this study are in agreement with those results. Both studies indicate the existence of significantly smaller magnitudes of vertical motion (when convection is absent) than is observed to be present in middle-latitude disturbances.

The question arises of exactly how non-horizontal and divergent is the flow in the easterly wave when cumulus heating is present. The parameterization schemes investigated tend to agree that even with the inclusion of latent heat, vertical motion and linkage of upper and lower tropospheric motion for the wave involved is quite small compared to middle latitude systems. Time mean rising motions behind the wave axis in each parameterization, with the exception of Experiments 4 and 5, were -6×10^{-4} mb sec^{-1} or less. This is recognized as a factor of 5 or more smaller than vertical motions in a middle latitude disturbance.

Ascending motion of -6 to -8×10^{-3} mb sec^{-1} was observed in Experiments 4 and 5. Experiments 4 and 5, however, show overdevelopment and -6 to -8×10^{-3} mbs^{-1} can be assumed to be significantly larger than that which actually did exist within the wave.

Conversions of eddy available potential energy to eddy kinetic energy as seen in Fig. 14 tend not to exceed 10^{-3} mb m sec^{-1}. Krishnamurti (1969), in a 24-hour prediction of the intertropical convergence zone, obtained conversion rates on the order of 10^{-2} mb m sec^{-1}. These values would indicate that this moderate intensity wave was a relatively small producer of eddy kinetic energy compared to the ITCZ. Experiments 4 and 5 which overdevelop the wave show conversion of potential to kinetic energy at rates comparable to those found in the ITCZ by Krishnamurti.

(a) *The cumulus heating role in producing vertical motion and eddy kinetic energy*

Recent studies, primarily diagnostic in nature, have raised the questions of what magnitudes of vertical motion are typical of tropical disturbances and what percent of the rising motion in a disturbance is the direct effect of cumulus heating. Baumhefner (1968), Erickson (1971), and others have obtained percentages of vertical motion produced by cumulus heating ranging from greater than fifty percent to less than two percent.

Parameterizations used in this study all suggest that, in the case of this non-developing easterly wave, release of latent heat by cumulus clouds was by far the primary physical process producing ascending motion. Since no ω-equation is used in the forecast, one cannot determine exactly the size of the cumulus heating forcing function; however, we can compare the vertical motion magnitudes with and without cumulus heating. In the Figs. 6*a*–12*a*, only the forecast without cumulus heating fails to have a well-defined cell of ascending air at mid-levels east of the wave axis. A crude estimate of the ratio of ascending motion without cumulus heating to ascending motion with cumulus heating would be on the order of one or two to ten for parameterizations tested. In the mid-levels east of the wave axis, omega is small and positive for Experiment 1 while being large and negative for the remaining experiments. For an explicit comparison, Fig. 15 contains vertical motion maps of Experiment 1 (no heating) and Experiment 3 (Yamasaki heating ($h = h(x, y, p, t)$) for 700 mb at forecast hour 18.

The possibility exists that all parameterizations are biased toward overheating and overproduction of ascending motion. Aside from the fact that all schemes have been previously used and have yielded reasonable results, evidence obtained from the comparative integrations indicates not all schemes are overheating. For example, Experiment 3 produces a better 1 000-mb forecast of height and wind than Experiment 2. In Experiment 2 the low-level system moves approximately 200 kilometers too far in 48 hours. The slower movement in Experiment 3 is traceable to the larger rising motion east of the wave axis. Increased low-level convergence produces more vorticity east of the wave axis and thereby retards the east to west transla-

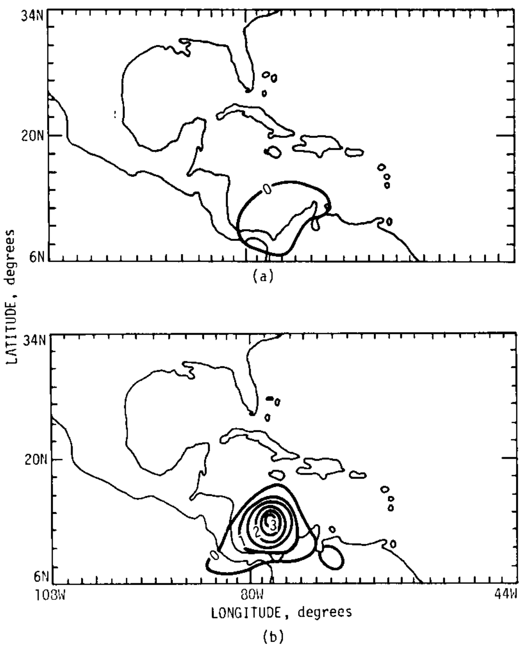

Fig. 16. Cumulus latent heating of the Krishnamurti and Moxim forecast in degrees θ per day, (*a*) forecast hour 3 and (*b*) forecast hour 24. Isopleth interval is 0.50 degrees θ per day.

tion. Experiment 2 apparently has insufficient heating to slow the wave movement.

The discrepancy between the percent of vertical motion produced by cumulus heating in diagnostic studies (5–50 %) and the estimated percent (70–80 %) involved in these comparative forecasts is perhaps explained by a closer look at the moisture distribution of the data involved. It is generally agreed that the moisture data in the tropics are not totally reliable, but for lack of better data, raw moisture values are utilized, usually with some smoothing. The parameterization schemes of several of the diagnostic studies have been similar to that of Krishnamurti & Moxim, which is extremely sensitive to the analyzed moisture field. The heating parameterized will be very small if the relative humidity does not approach saturation (Q_2 is dominant over Q_1 in Eq. (2.2)). This was the case in Experiment 2 where initial cumulus heating was near zero. For the first 9–12 forecast hours convection was being predicted, but the primary result was to bring the disturbed area to near saturation. Once the environment approached saturation, sensible heating took place at a rate comparable to that of the other experiments. Figs. 16*a* and *b* show Krishnamurti & Moxim heating rates in degrees θ per day at 700 mb for forecast hours 3 and 24. Ascending motion produced by the heating of Figs. 16*a* and *b* varies accordingly. In a diagnostic study, if the parameterization were similar to that of Krishnamurti & Moxim, heating rates would resemble those of Fig. 16*a* unless the initial relative humidities were analyzed to near 100 %.

Conversions of eddy kinetic energy from eddy available potential energy reflect, as do the vertical motion fields, the dominant effect of cumulus heating in the six forecasts which include it. As mentioned previously, in Figs. 13*a* and *b*, the forecast with no heating shows by far the lowest production rate of eddy kinetic energy. Most eddy kinetic energy production rates for experiments including heating are nearly an order of magnitude larger than that with no heating. At latitudes 14°–18° N, experiments including cumulus heating show production of kinetic energy while Experiment 1 shows destruction of kinetic energy.

6. Summarizing comments on each experiment and conclusions

In examining large volumes of generated data in the seven forecasts, the author has taken note of some of the particular characteristics of each of the parameterization schemes. Items of particular interest are summarized in the following subsections.

(a) *Experiment 1, no cumulus heating*

The forecast made with no latent heat release has re-emphasized the suggestion of Charney (1963) that the tropics, excepting intense tropical storms and away from the inter-tropical convergence zone, are very nearly barotropic in nature. Tropical systems have been forecast with considerable skill without including latent heat release. Primary weaknesses of the forecast with no cumulus heating were: the forecasting of too rapid movement of the low-level wave, and the lack of an internal cell of ascending motion within the wave. Maintenace of kinetic energy levels without a significant ascending cell in the wave is not possible because the frictional dissipation exceeds the conversion of eddy kinetic energy from eddy available potential energy.

(b) *Experiment 2, Krishnamurti & Moxim*

Krishnamurti & Moxim heating yields a very realistic static energy forecast by inclusion of the cumulus scale mixing of moisture from cloud to environment. Weaknesses of this scheme include its sensitivity to the initial moisture distribution and the tendency to produce insufficient heating due to the Q_2 term in Eq. (2.2). Underheating is indicated by overly rapid movement of the low-level easterly wave.

(c) *Experiment 3, Yamasaki* ($h = h(x, y, p, t)$)

Yamasaki heating produces a forecast which must be considered as one of the best of the seven made. The low levels are heated by amounts of two to three times that of Experiment 2 and the corresponding translation of the low-level wave was less. Furthermore, the larger heating of this scheme was more nearly able to maintain the kinetic energy of the wave than had the heating of Experiment 2.

One shortcoming of the Yamasaki scheme is the lack of cumulus moisture mixing from cloud to environment as exists in Krishnamurti & Moxim heating. Obviously, since no moisture was predicted in the Yamasaki integration model, there was no need for the mixing term. The inclusion of the $(q_c - q)$ term in this scheme would be simple and straightforward.

(d) *Experiments 4 and 5, Yamasaki* ($h = h(p)$)

Experiments 4 and 5 were the poorest of the seven forecasts in terms of verification. Both forecasts displayed local overdevelopment in the region of strongest convection. The overdevelopment in each case was determined to be the result of the unconditional heating function ($h = h(p)$). Unrealistic quantities of latent heat continued to be added even though the environment was warmer than the cloud. The result was that total heating over a period of 48 hours was several factors larger than that of Experiment 3 ($h = h(x, y, p, t)$).

The simple heating function $h = h(p)$ was specifically designed for symmetric hurricane studies. Because the latent heating cannot adjust to the large scale variables in either time or space, the broader application of this scheme to real data forecasting does not appear to have merit.

The tropical linear perturbation analysis of Yamasaki (1969) can be questioned because of the unrealistically large latent heating involved in the nonceasing convection.

(e) *Experiment 6, convective adjustment*

Vertical motions of this experiment were comparable in magnitude to those of forecasts using the other parameterizations. However, they are somewhat smaller than that typically found in general circulation studies in the tropics. This is explained by the lack of any large area of saturated air in the initial data. General circulation forecasted fields, on the other hand, tend to have rather large and continuous regions of saturation. The convection area that evolved in this experiment was not extensive.

A considerable portion of the convection that did occur was related to large moisture values in the initial data rather than the initial motion disturbance. Low level vorticity was produced in an area removed from the initial disturbance and consequently the low level motion field became less organized. The necessary link between the motion disturbance and total saturation implied in this scheme indicates the scheme to be less desirable for real data forecasting.

(f) *Experiment 7, cumulus scale mass conservation*

This scheme has a difficulty similar to one found in Experiment 6. In this case, if maximum low-level moisture is not completely coincident with the disturbance, the scheme will have a tendency to produce a disturbance in the area of maximum low-level moisture. Vertical motions appear realistic in magnitude but are also displaced in the horizontal.

Moisture was predicted only in the lowest level of the Mintz–Arakawa general circulation model. A difficulty was encountered in Experiment 7 when moisture was predicted at four levels. Moisture below 300 mb was continuously depleted by cumulus scale subsidence. Some type of cloud-environment mixing in mid- and low-levels would be necessary to counter this unrealistic drying.

(g) *Conclusions*

Six forecasts were made that included release of cumulus latent heat. Only those involving a time-independent vertical heat release function (Yamasaki, 1968*a*, 1969) produced unacceptable forecasts. In these two forecasts (Experiments 4 and 5), overheating occurred, followed by overdevelopment of the easterly wave. Forecasts using parameterizations of Krishnamurti & Moxim (1971), Yamasaki (1968*c*) with time-dependent heat release function, convective adjustment, and cumulus scale mass conservation, produced forecasts of a similar nature. Deviations of pressure-level heights among these forecasts did not, in general, exceed 10 metres at a particular grid point. Mean maximum ascending motions in the vicinity of the easterly wave ranged from a low of -2×10^{-4} mb sec^{-1} in the Krishnamurti & Moxim experiment to a high of near -6×10^{-4} mb sec^{-1} in the Yamasaki experiment. Mean vertical motions predicted in the two cases of excessive easterly wave development were as large as -3×10^{-3} mb sec^{-1}.

The Krishnamurti & Moxim parameterization produced better fields of total static energy $(gz + c_pT + Lq)$ but showed evidence of underheating. The low-level ascending motion produced by Krishnamurti & Moxim heating east of the wave axis did not produce sufficient low-level vorticity to slow the wave movement. The wave was forecast to move approximately 200 km too far in 48 hours. Yamasaki heating with a time dependent heat release function produced more low-level vorticity east of the wave axis and consequently a better low-level forecast resulted.

Convective adjustment and cumulus scale mass conservation appear to be less desirable for real data forecasting if the data show large amounts of moisture and saturation not perfectly coincident with the motion disturbance. Areas of high saturation in forecasts made with these two schemes experienced strong latent heating and the induced vertical motion there produced a moisture-related disturbance. The result was that a secondary maximum of vorticity developed in the moist region and the wave tended to become disorganized.

Excepting the two forecasts which contained obvious overheating and system overdevelopment, all predictions tend to substantiate Charney's (1963) scale analysis of tropical motions; i.e., except for intense tropical storms and the inter-tropical convergence zone, tropical motions are quasi-nondivergent with upper and lower tropospheric motions nearly uncoupled. Vertical coupling produced by parameterized cumulus latent heat release in this wave of weak-to-moderate intensity could be classified at most as being small compared to extratropical wave disturbances. Maximum vertical motions predicted in Experiments 1, 2, 3, 6 and 7 are on the order of $4\text{–}8 \times 10^{-4}$ mbs^{-1} outside convective areas and -2×10^{-3} mb sec^{-1} in regions of strongest cumulus heating. Appreciable coupling did occur in the cases of overheating (Experiments 4 and 5). The strong coupling, however, must be regarded as not being characteristic of the true wave since overdevelopment did take place in the forecasts.

Of the ascending motion and eddy kinetic energy produced within the easterly wave, an estimated 70–80 % could be directly attributed to cumulus latent heat release. In the case of no latent heat release, vertical motion fields displayed no continuous ascending region east of the wave axis in mid-levels, and correspondingly, production rates of eddy kinetic energy were the lowest of all forecasts made.

Acknowledgements

The author is grateful for the continuous advice and suggestions of Dr T. N. Krishnamurti. Thanks also to Lois Gries and Cathy Ellison for the manuscript typing and to Denise Ellingson, Dewey Rudd, and Marc Jordan for drafting and photographing the figures.

Financial support was provided by the National Science Foundation under Grant NSF GA-17822.

Computational support was provided in part by the Florida State University Departments of Meteorology and Computer Science. Acknowledgement is also made to the National Center for Atmospheric Research, which is sponsored by the National Science Foundation, for use of its Control Data 6600 and 7600 computers.

REFERENCES

Arakawa, A., Katayama, A. & Mintz, Y. 1969. Numerical simulation of the general circulation of the atmosphere. *Proceedings of the WMO/IUGG Symposium on Numerical Weather Prediction*, Tokyo.

Baumhefner, D. P. 1968. Application of a diagnostic model to the tropical atmosphere. *Mon. Wea. Rev. 96*, 218–228.

Charney, J. G. 1963. A note on large-scale motions in the tropics. *J. Atmos. Sci. 26*, 182–185.

Charney, J. G. & Eliassen, A. 1964. On the growth of the hurricane depression. *J. Atmos. Sci. 21*, 68–75.
Erickson, C. O. 1971. Diagnostic study of a tropical disturbance. *Mon. Wea. Rev. 99*, 67–78.
Jordan, C. L. 1958. Mean soundings for the West Indies area. *J. Meteor. 15*, 91–97.
Krishnamurti, T. N. 1968. A calculation of percent area covered by convective clouds from moisture convergence. *J. Appl. Met. 7*, 184–195.
Krishnamurti, T. N. 1969. An experiment in numerical prediction in equatorial latitudes. *Quart. J. Roy. Met. Soc. 95*, 594–620.
Krishnamurti, T. N. & Moxim, W. 1971. On parameterization of convective and non-convective latent heat release. *J. Appl. Met. 10*, 3–13.
Krishnamurti, T. N., Kanamitsu, M., Ceselski, B. F.& Mathur, M. B. 1972. F.S.U. Tropical Prediction Model: Report no. 72–1. Department of Meteorology, Florida State University.
Krishnamurti, T. N. & Kanamitsu, M. 1972. A study of a coasting easterly wave. Report no. 72–1, Dept. Meteorology, Florida State University.
Kuo, H. L. 1965. On formation and intensification of tropical cyclones through latent heat release by cumulus convection. *J. Atmos. Sci. 22*, 40–63.
Langlois, W. F. & Kwok, H. C. W. 1970. *Numerical simulation of weather and climate, part III. Hyperfine grid with improved hydrological cycle.* IBM Research Laboratory, San Jose, Calif.
Manabe, S., Smagorinsky, J. & Strickler, R. F. 1965. Simulated climatology of a general circulation model with a hydrological cycle. *Mon. Wea. Rev. 93*, 769–798.
Ooyama, K. 1964. A dynamical model for the study of tropical cyclone development. *Geofis. Intern. 4*, 187–198.
Ooyama, K. 1969. Numerical simulation of the life cycle of tropical cyclone. *J. Atmos. Sci. 26*, 3–40.
Riehl, H. 1954. *Tropical meteorology.* McGraw-Hill, New York.
Rosenthal, S. L. 1969. Numerical experiments with a multi-level primitive equation model designed to simulate the development of tropical cyclones, Experiment I. *ESSA Technical Memorandum ERLTM-NHRL, No. 82.*
Shukla, J. 1969. A numerical experiment on a disturbance in the tropical easterlies. *J. Met. Soc. Japan 47*, 109–114.
Washington, W. M. & Kasahara, A. 1970. A January simulation experiment with the two-layer version of the NCAR global circulation model. *Mon. Wea. Rev. 96*, 559–580.
Yamasaki, M. 1968*a*. Numerical simulation of tropical cyclone development with the use of primitive equations. *J. Met. Soc. Japan 46*, 178–201.
Yamasaki, M. 1968*b*. A tropical cyclone model with parameterized vertical partition of released latent heat. *J. Met. Soc. Japan 46*, 202–214.
Yamasaki, M. 1968*c*. Detailed analysis of a tropical cyclone simulated with a 13-layer model. *Papers in Meteorology and Geophysics 20*, 289–336.
Yamasaki, M. 1969. Large-scale disturbances in the conditionally unstable atmosphere in low latitudes. *Papers in Meteorology and Geophysics 19*, 559–585.

СРАВНЕНИЕ СХЕМ ПАРАМЕТРИЗАЦИИ КОНВЕКТИВНОЙ ОБЛАЧНОСТИ

Для исследования существующих схем параметризации конвективной облачности используется улучшенная модель, основанная на примитивных уравнениях и квазилагранжевых переменных. Сравнение проводится для 48-часовых прогнозов с использованием семи различных функций нагревания, одна из которых подразумевает, что скрытая теплота в облаке равна нулю. В качестве начальных данных принята неразвивающаяся восточная волна в Карибском море.

Из шести прогнозов, использовавших скрытую теплоту, два, включавших не зависящую от времени вертикально распределенную функцию нагревания, оказались наиболее ошибочными. Параметризация нагревания по Кришнамурти и Моксиму, а также по Ямасаки с зависящей от времени функцией высвобождения тепла по вертикали, с конвективными приспособлением и сохранением массы в масштабе облака, приводит к сравнимым результатам. Средние максимальные восходящие движения для четырех подобных прогнозов измеряются от -20×10^{-4} *мб* сек$^{-1}$ для модели Кришнамурти и Моксима до -6×10^{-4} *мб* сек $^{-1}$ для модели Ямасаки. Модели с конвективным приспособлением и сохранением массы в масштабе облака приводят к худшим прогнозам для нижних уровней из-за сильной зависимости от начального распределения влажности.

Результаты прогнозов согласуются с масштабным анализом Чарни процессов в тропиках. Для восточной волны умеренной интенсивности вычисленные вертикальные движения не указывают на взаимосвязь движений в верхней и нижней тропосфере вне конвективных зон и дают минимальную связь в областях освобождения скрытого тепла в облаках. От семидесяти до восьмидесяти процентов восходящего движения и вихревой кинетической энергии, возникающих внутри волны, являются, согласно оценкам, прямым результатом параметризации скрытого тепла в облаках.